^{13}C-NMR study of charge fluctuations in α-(BEDT-TTF)MX salts (M = alkali metal; X = S, Se)

Akihiro Ohnuma and Atsushi Kawamoto

Department of Condensed Matter Physics, Graduate School of Science, Hokkaido University, Sapporo 060-0810, Japan

(Received 12 June 2019; revised manuscript received 1 November 2019; published 4 December 2019)

Optical studies of the density wave (DW) salt of α-(BEDT-TTF)$_2$KHg(SCN)$_4$ revealed a pseudogap due to a charge fluctuation below $T^* \simeq 200$ K. Moreover, ^{13}C-NMR studies of the DW salt of α-(BEDT-TTF)$_2$RbHg(SCN)$_4$ and of the superconductivity (SC) salt of α-(BEDT-TTF)$_2$NH$_4$Hg(SCN)$_4$ suggested that the NMR line width of the A site increased and the charge disproportionation in the A column developed below T^*. These phenomena may be due to the development of a horizontal stripe modulation of the local charge density. However, whether the horizontal stripe modulation develops or not and the relationships among T^* anomalies, the pseudogap, and line broadening, were unclear. In this study, ^{13}C-NMR measurements were obtained of the metallic salt of α-(BEDT-TTF)$_2$TlHg(SeCN)$_4$, and its electronic structure was compared with those of the DW and SC salts. The NMR line width of the A site and χ_B/χ_C in Rb(SCN) and NH$_4$(SCN) increased and deviated from that in Tl(SeCN) below T^*, suggesting the development of the instability of horizontal stripe modulation in Rb(SCN) and NH$_4$(SCN) and that T^* anomalies could be due to the instability.

DOI: 10.1103/PhysRevB.100.245107

I. INTRODUCTION

Superconductivity is frequently realized near the insulating phase due to strong electronic correlations. For example, charge fluctuations and antiferromagnetic spin fluctuations are thought to contribute to the superconductivity of cuprate superconductors. The BEDT-TTF family of organic conductors has also shown superconductivity near the insulating phase. Half-filled organic superconductors κ-(BEDT-TTF)$_2X$ are somewhat similar to cuprate superconductors and heavy fermion compounds. In the phase diagrams of κ-(BEDT-TTF)$_2X$, the superconducting (SC) phase is adjacent to the antiferromagnetic insulating phase with a tuning parameter of effective electronic correlations U/W, where U and W are the on-site Coulomb repulsion and bandwidth, respectively. In the κ-(BEDT-TTF)$_2X$ system, superconductivity may be mediated by spin fluctuation [1]. In some quarter-filled BEDT-TTF salts, however, superconductivity is also realized near the ordered state of charge degrees of freedom. In these quarter-filled systems, V/W, in which V is the off-site Coulomb repulsion, could be significant and realizes a spontaneous inhomogeneity such as horizontal, stripe, and checkerboard charge ordering (CO) (Fig. 1) [2,3]. This instability is considered to mediate the superconductivity [4,5].

The family of quarter-filled organic conductors, α-(BEDT-TTF)$_2M$Hg(XCN)$_4$ [abbreviated M(XCN), in which M = Tl, K, Rb, or NH$_4$ and X = S or Se], is one of the best candidates to study superconductivity in quarter-filled systems [6]. α-(BEDT-TTF)$_2M$Hg(XCN)$_4$ compounds possess 1D and 2D Fermi surfaces and shows a metal-like behavior at high temperatures. These compounds differ at low temperatures, with NH$_4$(SCN) showing the SC state at about 1.5 K [7,8], whereas Tl(SCN), K(SCN), and Rb(SCN) showed anomalies at about 10 K. Below this temperature, no enhancement of $1/T_1T$ was observed [9,10], and the Fermi surface was observed to be reconstructed in angular dependent magnetoresistance oscillations, suggesting that the DW state is due to a nesting instability [11–13].

Additional anomalies have been reported around $T^* \simeq 200$ K. Optical studies of K(SCN) showed that a pseudogap developed below T^*. This pseudogap may have been due to a charge fluctuation, which, in turn, may contribute to superconductivity [14,15].

To investigate this charge disproportionation, site-selective ^{13}C-NMR measurements of Rb(SCN) and NH$_4$(SCN) were performed [16,17]. Because three nonequivalent molecules were involved, consisting of A, B, and C in α-type salts, the local electronic properties of each molecule could be determined. Below $T^* \simeq 200$ K, the line width of the A molecule increased, suggesting the development of a disproportionation in A molecules. This disproportionation in A molecules, along with infrared vibrational spectroscopy, suggested that inversion symmetry resulted in the breaking of A molecules [18]. The inhomogeneity between B and C molecules also increased with decreasing temperature, a phenomenon that may be due to the development of horizontal stripe modulation below T^*, which means that B and C molecules become charge rich and poor sites, respectively, and A molecules also become charge rich and poor sites due to the inversion symmetry breaking. Actually, it was reported from x-ray diffraction (XRD) measurement that the horizontal stripe CO was realized in α-(BEDT-TTF)$_2$I$_3$ and θ-type salts [19,20], which have same and similar BEDT-TTF molecular arrangement as α-(BEDT-TTF)$_2M$Hg(XCN)$_4$, respectively. In β''-SF$_5$$RSO_3$ (R = CH$_2$, CHFCF$_2$, CH$_2$CF$_2$, and CHF), the checkerboard and vertical stripe CO were observed in R = CH$_2$ and CHFCF$_2$, respectively, and the superconductivity was realized in R = CH$_2$CF$_2$. The V/W phase diagram was suggested from dc transport and optical experiments where the superconductivity could be mediated by the charge fluctuation [21–23]. Theoretical studies also

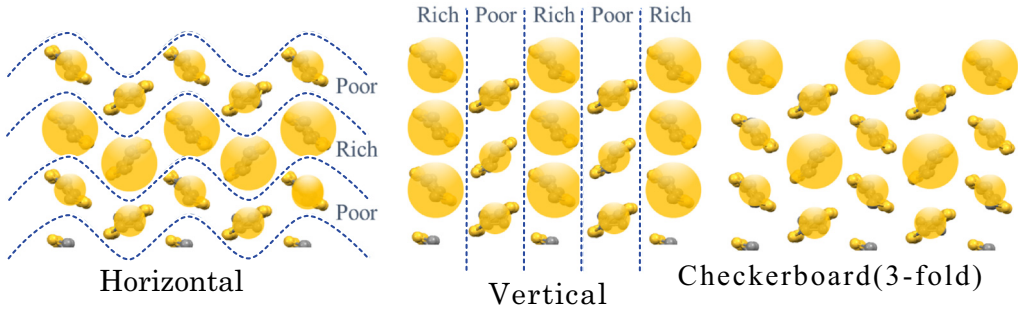

FIG. 1. Charge patterns of BEDT-TTF salts.

pointed out that a charge frustration enhanced by the checkerboard charge pattern induces the d_{xy}-wave paring superconductivity at quarter filling [5], suggesting there is the relationship between a charge pattern and paring mechanism of the superconductivity. However, because no anomaly due to the inhomogeneity between B and C molecules was observed below T^* in Rb(SCN) and NH_4(SCN), it was unclear about the charge pattern and whether horizontal stripe modulation develops below T^* [17]. To clarify the relationships among T^* anomalies, systematic NMR evaluation is needed of a reference salt that behaves as a simple metal on the phase diagram.

Although universal phase diagrams have been obtained of κ, θ, and β''-type salts and of quasi-1D TMTCF salts, phase diagrams of α-type salts remain unclear. The phase diagrams of organic conductors were simply tuned by hydrostatic pressure or chemical modification, whereas phase diagrams may be obtained by measuring resistivity under conditions of uniaxial strain [24]. Assessments of uniaxial strain along the conducting a-c plane showed that the c-axial strain alters the DW state of Rb(SCN)to an SC state, whereas the a-axial strain alters the SC state of NH_4(SCN) to the DW state, suggesting the proposed c/a phase diagram.

However, the uniaxial strain method was unsuitable for NMR studies on the phase diagram as pressure cells restrict the direction of the field and prevents the ability to acquire separated NMR spectra. Chemical pressure may be more suitable to systematic NMR analyses. Recently, NH_4(SeCN) was found to be in the DW state and to link the X = S system to the X = Se system [25]. In comparison, Tl(SeCN) was found to be in a simple metallic phase without a DW anomaly [26]. These findings enable systematic NMR evaluation and comparisons of the electronic structure of simple metallic states of X = Se salts with the DW and SC states of X = S salts.

This present study utilized ^{13}C-NMR measurements of the metallic salt of Tl(SeCN) and compared its electronic structure with the structures of Rb(SCN) and NH_4(SCN). These comparisons revealed the relationships among T^* anomalies, including pseudogaps and line broadening.

II. EXPERIMENTAL

A single crystal of the Tl(SeCN) was prepared with the electrochemical oxidation method. In this molecule, one side of the central C=C bond was selectively enriched with ^{13}C to prevent the NMR peak splitting due to the Pake doublet [Fig. 2(a)] [27]. NMR spectra were obtained using a spin-echo method with an external magnetic field of 6.1 T. The angular dependence of the NMR shift was measured with rotation around b^* axis ($\theta = 0°$: a axis, $\theta = 90°$: $c' = a \times b^*$ axis). Because the hyperfine coupling constants of A and B, C molecules are large at $\theta = 54°$ and $\theta = 127°$ [16], the line widths and NMR shifts of A, B, and C sites were measured at $\theta = 54°$ and $\theta = 127°$, respectively. Atomic parameters of α-type salts, Rb(SCN), NH_4(SCN), and Tl(SeCN), needed to estimate local spin susceptibilities from NMR shifts were assessed with XRD measurements (Rigaku R-AXIS RAPID) with Mo K-α radiation of $\lambda = 0.71075$ Å.

III. RESULTS AND DISCUSSIONS

A. Site assignment and determination of hyperfine coupling constant

The α-type salts contain three nonequivalent BEDT-TTF molecules, A, B, and C [Fig. 2(b)], with the A molecule located in a general position and B and C molecules located in the inversion center. Because the carbon atoms of the central C=C bond on the A molecule are crystallographically nonequivalent, whereas those on the B and C molecules are equivalent, the nonequivalent ^{13}C sites, A_a, A_b, B, and C, appeared as four NMR peaks (Fig. 3, inset). As the NMR shift is maximal when the external field is parallel to the p_z orbital, these NMR peaks could be assigned by the angular dependence of the NMR shifts. Figure 3 shows the angular dependence of the NMR shift of Tl(SeCN) around the b^* axis at 250 K. The horizontal axis is the angle of the external field from the a axis ($\theta = 0°$) to the c' axis ($\theta = 90°$). The curves for the closed black circles, the red squares, the blue triangles, and the pink inverted triangles were assigned to the A_a, A_b, B, and C sites, respectively.

The NMR shift can be expressed using the equation $\delta(\theta) = K_{spin}(\theta) + K_{vv}(\theta) + \sigma(\theta)$, where θ is the field direction from the a axis to the c'axis, $K_{spin}(\theta)$ is a spin term of the Knight shift, $K_{vv}(\theta)$ is a Van Vleck term of the Knight shift, and $\sigma(\theta)$ is a chemical shift. As for BEDT-TTF compounds, the Van Vleck term is negligible because the splitting in the energy levels between the $2p_z$ orbital of the central C=C bond (π) and unoccupied $2p_x$, $2p_y$ orbitals (σ^*) is large and the secondary perturbation is significant small unlike the cuprate compounds, which have almost degenerate states due to the small crystal field [28]. Hence, we can neglect the Van Vleck

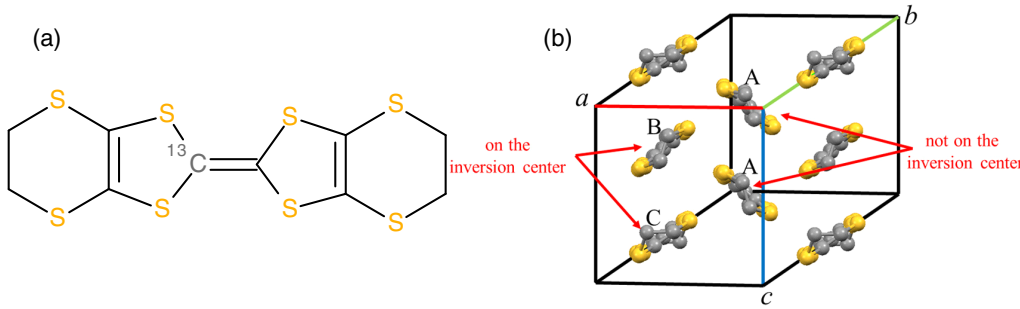

FIG. 2. (a) Molecular structure of BEDT-TTF. The molecule was selectively enriched in ^{13}C to prevent the Pake doublet effect. (b) Donor layer of α-type salts viewed along the b axis.

term, and the NMR shift is described as $\delta(\theta) \simeq K_{\rm spin}(\theta) + \sigma(\theta) = A(\theta)\chi_{\rm s} + \sigma(\theta)$, where $\chi_{\rm s}$ is a local spin susceptibility and $A(\theta)$ is a hyperfine coupling constant.

The chemical shift could be estimated from the chemical shift tensor for $(\text{BEDT-TTF})^{+0.5}$ molecule [29]. The angular dependence of the Knight shift for each site could be calculated by subtracting the chemical shift from the observed NMR shift. The temperature dependence of the local spin susceptibilities, $\chi_{\rm s}$, could be determined by measuring a Knight shift large enough to be observed. The angles θ most suitable for the A and the B and C sites were found to be 54° and 127°, respectively (Fig. 3, dashed line). Therefore, to evaluate local spin susceptibilities, it was necessary to determine the hyperfine coupling constants at the corresponding angles.

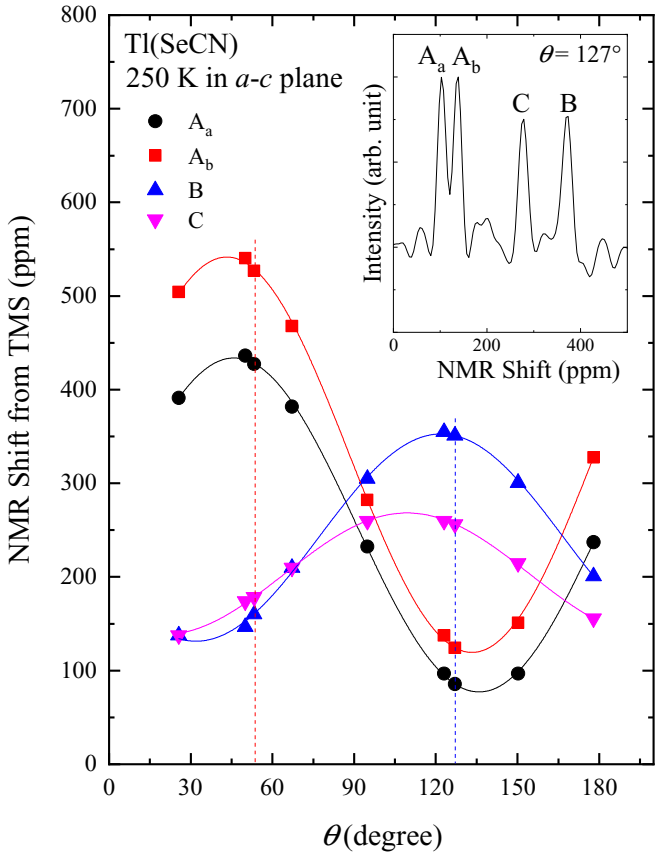

FIG. 3. Angular dependence of the NMR shift of the Tl(SeCN) around the b^*axis at 250 K. The dashed lines denote the field direction of the $\theta = 54°$ and 127°. The inset shows the NMR peaks of each nonequivalent ^{13}C site, A_a, A_b, B, and C at θ =127°.

Hyperfine coupling constants were determined with the following analysis. The anisotropy of the Knight shift mainly depends on the anisotropy of the hyperfine coupling constant, which is primarily due to the p_z orbital of the BEDT-TTF molecule. Thus, the amplitude of the Knight shift is likely proportional to the local spin susceptibility. The ratios of local spin susceptibility determined from the angular dependence of the Knight shift [30] could be expressed as $\chi_{\rm A}$(250 K):$\chi_{\rm B}$(250 K):$\chi_{\rm C}$(250 K) = 1:0.66:0.46, with the amplitude at the A site being the mean of the amplitudes of the $A_a$and A_b peaks, and with the amplitudes of the B and C peaks. From total spin susceptibilities measured using a SQUID magnetometer [$\chi_{\rm SQUID}=\frac{1}{2}\chi_{\rm All}=\frac{1}{2}(2\chi_{\rm A}+\chi_{\rm B}+\chi_{\rm C})$] [25], we estimated the local spin susceptibilities to be $\chi_{\rm A}$ (250 K) = 6.7×10^{-5} emu/mol, $\chi_{\rm B}$ (250 K) = 4.4×10^{-5} emu/mol, and $\chi_{\rm C}$ (250 K) = 3.1×10^{-5} emu/mol. Using the chemical shift of 59.8 ppm for A site at 54° and those of 60.2 ppm for the B site and 58.3 ppm for the C site at 127°, the hyperfine coupling constants of Tl(SeCN) were determined to be $A_{\rm Aa}$= 15.2 kOe/$\mu_{\rm B}$ and $A_{\rm Ab}$= 19.4 kOe/$\mu_{\rm B}$ at $\theta = 54°$, $A_{\rm B}$= 18.4 kOe/$\mu_{\rm B}$, and $A_{\rm C}$= 17.7 kOe/$\mu_{\rm B}$ at θ = 127°. Because the atomic parameters of Rb(SCN) have not been determined, the chemical shift for Rb(SCN) was previously calculated using the atomic parameters of NH_4(SCN) [16]. For systematic comparisons, however, the corresponding atomic parameters should be used. Hence XRD measurements for Rb(SCN) and NH_4(SCN) were taken, and the chemical shifts of Rb(SCN) and NH_4(SCN) were evaluated using the following atomic parameters: For Rb(SCN), 59.4 ppm for the A site at 54°, 60.3 ppm for the B site at 127°, and 58.6 ppm for the C site at 127°; for NH_4(SCN), 59.9 ppm for the A site at 56°, 62.6 ppm for the B site at 142°, and 68.0 ppm for the C site at 142°. For Rb(SCN), the hyperfine coupling constants were determined to be $A_{\rm Aa}$ = 13.1 kOe/$\mu_{\rm B}$ and $A_{\rm Ab}$ = 14.8 kOe/$\mu_{\rm B}$ at $\theta = 54°$, $A_{\rm B}$ = 14.7 kOe/$\mu_{\rm B}$, and $A_{\rm C}$ = 14.0 kOe/$\mu_{\rm B}$ at θ = 127°, whereas for NH_4(SCN), these constants were determined to be $A_{\rm Aa}$ = 12.8 kOe/$\mu_{\rm B}$ and $A_{\rm Ab}$ = 14.2 kOe/$\mu_{\rm B}$ at $\theta = 56°$, $A_{\rm B}$ = 13.7 kOe/$\mu_{\rm B}$, and $A_{\rm C}$ = 11.7 kOe/$\mu_{\rm B}$ at θ = 142°. NMR parameters of α-$(\text{BEDT-TTF})_2M\text{Hg}(X\text{CN})_4$ are summarized in Table I.

TABLE I. NMR parameters of α-(BEDT-TTF)$_2M$Hg(XCN)$_4$.

	θ	^{13}C site	δ (ppm)	σ (ppm)	K (ppm)	χ (250 K) (10^{-5} emu/mol)	A (kOe/μ_B)
NH_4(SCN)	56°	A_a	441.5 [17]	59.9	381.6	16.6	12.8
	56°	A_b	554.0 [17]	59.9	494.1	19.4	14.2
	142°	B	368.1 [17]	62.6	305.5	12.5	13.7
	142°	C	283.0 [17]	68.0	215.0	10.3	11.7
Rb(SCN)	54°	A_a	426.5 [16]	59.4	367.1	15.6	13.1
	54°	A_b	540.2 [16]	59.4	480.8	18.1	14.8
	127°	B	369.2 [16]	60.3	309.0	11.8	14.7
	127°	C	305.8 [16]	58.6	247.3	9.83	14.0
Tl(SeCN)	54°	A_a	426.7	59.8	366.9	12.6	15.2
	56°	A_b	526.9	59.8	467.1	14.3	19.4
	127°	B	350.9	60.2	290.7	8.83	18.4
	127°	C	256.3	58.3	198.0	6.25	17.7

B. Temperature dependence of local spin susceptibilities

The temperature dependence of the NMR spectrum of Tl(SeCN) was determined at $\theta = 54°$and 127° (Fig. 4). This spectrum enabled a determination of the temperature dependence of NMR shift for each peak (Fig. 5). The NMR shifts of A_a, A_b, B, and C show different temperature dependence. Because the NMR shifts mainly reflect the local density of state [31], this behavior suggests that the B and C molecules could become the charge-rich and -poor sites due to the off-site Coulomb repulsion, respectively. Based on the estimated hyperfine coupling constants, the local spin susceptibilities could be determined. We also evaluated the local spin susceptibilities of Rb(SCN) and NH_4(SCN) using reported temperature dependence of NMR shifts [16,17] and the hyperfine coupling constants described in Sec. III A. Figure 6(a) shows the temperature dependence of total spin susceptibilities ($\chi_{All} = 2\chi_A + \chi_B + \chi_C$), and Figs. 6(b)–6(d) shows the ratios of local spin susceptibilities (χ_i/χ_{All}; i = A, B, and C) of Tl(SeCN), compared with those of NH_4(SCN) and Rb(SCN). Here $\chi_A$is the average spin susceptibilities of the $A_a$and A_b sites, with χ_A estimated from the NMR shift of the A site at $\theta = 54°$, and χ_B and χ_C estimated from the NMR shifts of the B and C sites at $\theta = 127°$. The total spin susceptibilities of Tl(SeCN) measured with a SQUID magnetometer (χ_{SQUID}) were denoted by black stars in Fig. 6(a). The χ_{All} of Tl(SeCN) was consistent with its χ_{SQUID}.

The χ_A/χ_{All} showed almost the same temperature dependence, whereas χ_{All} showed different temperature

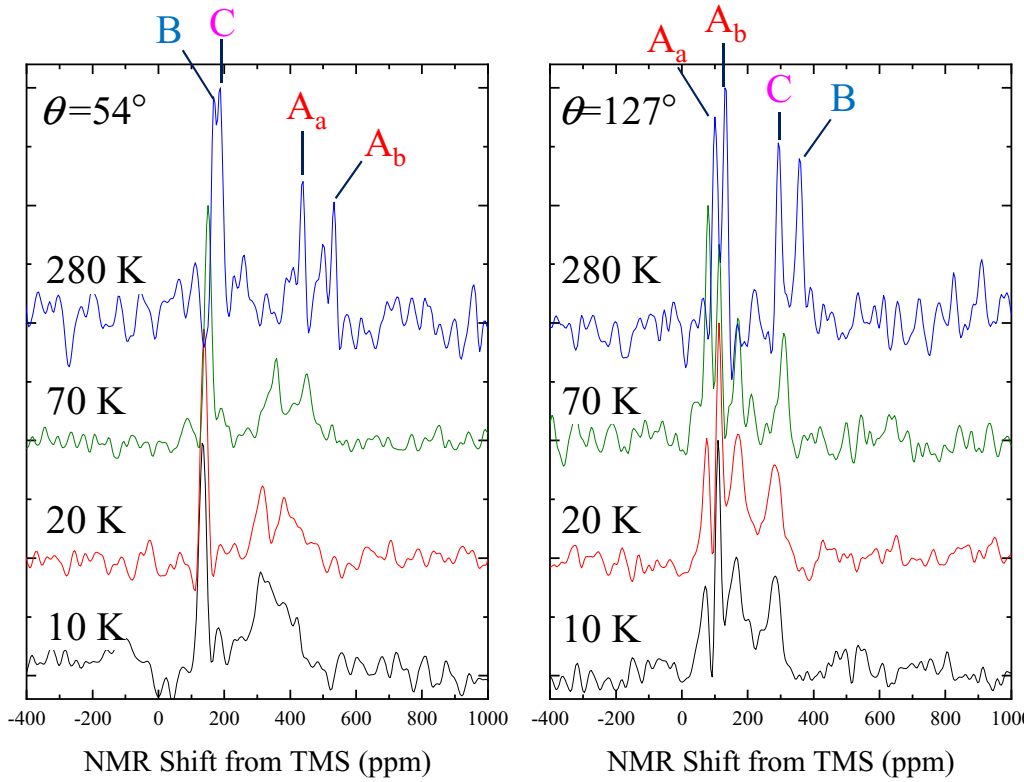

FIG. 4. NMR spectrum of Tl(SeCN) with $\theta = 54°$ and 127° at several temperatures.

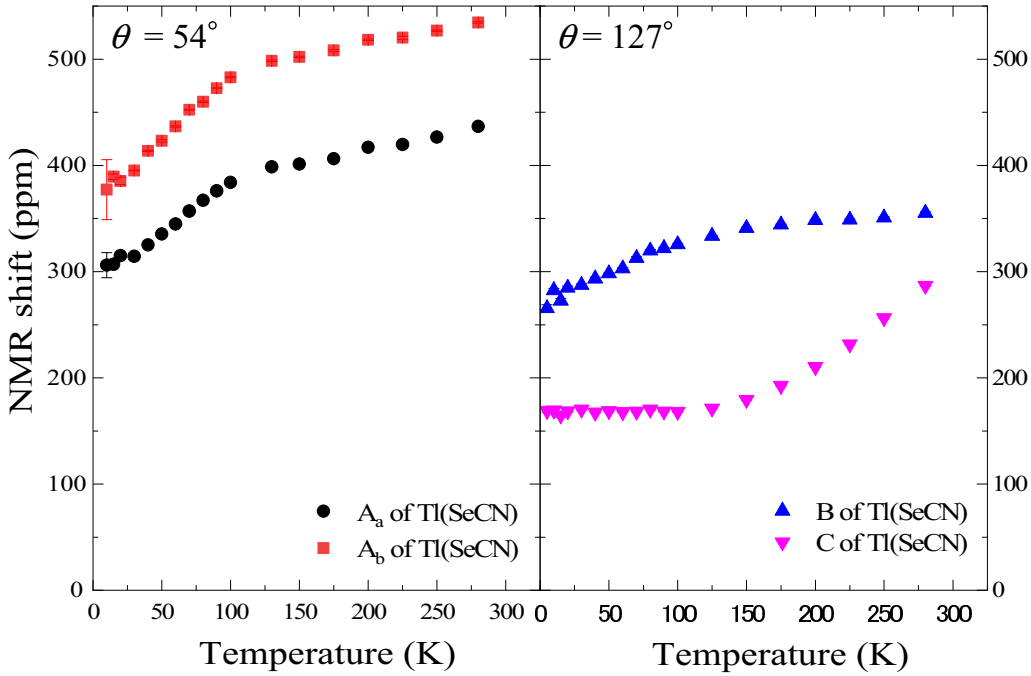

FIG. 5. Temperature dependence of the NMR shift of Tl(SeCN). The NMR shift of the $A_a$and A_b sites were measured at $\theta = 54°$ and those of the B and C sites at $\theta = 127°$. The error bars indicate the uncertainty of the fits.

dependences. At low temperatures, χ_B/χ_{All} ratios of $NH_4(SCN)$, Rb(SCN), and Tl(SeCN) differed significantly, with the χ_B/χ_{All} ratio of Tl(SeCN) being the smallest. The χ_C/χ_{All} ratio showed the opposite behavior at the B site, with the χ_C/χ_{All} ratio of Tl(SeCN) being the largest.

Previous ^{13}C-NMR studies suggested that the χ_B/χ_A ratio at low temperature could tune the ground state of α-type salts [17]. The $\chi_B/\chi_A$of Tl(SeCN) was 0.7, much smaller than those of Rb(SCN) and $NH_4(SCN)$, which were 0.9.

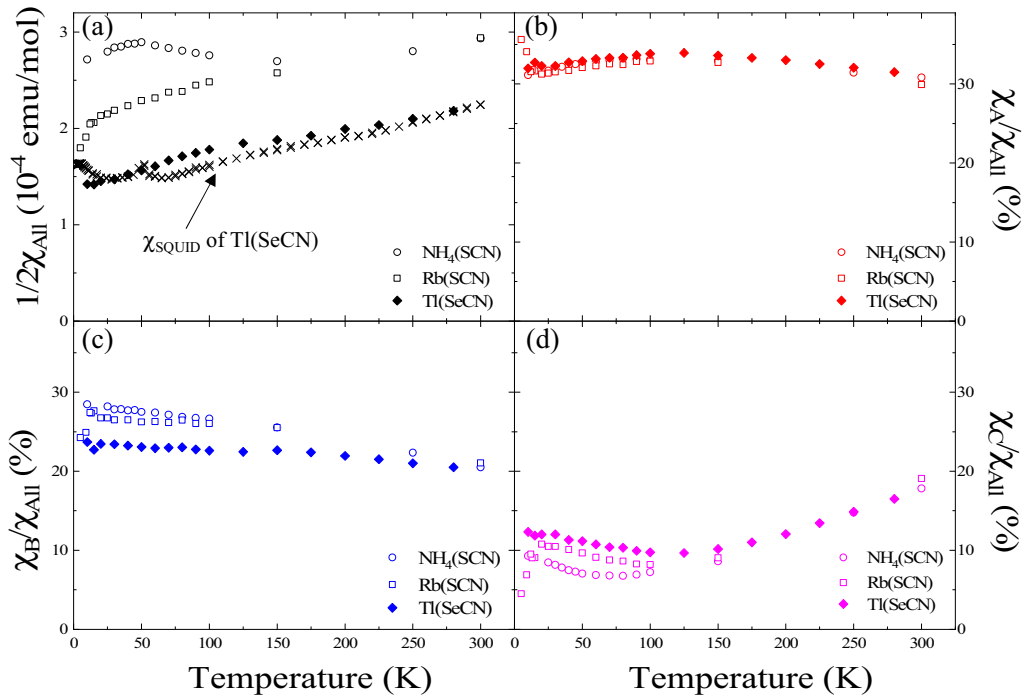

FIG. 6. Temperature dependence of (a) total spin susceptibilities ($\chi_{All} = 2\chi_A + \chi_B + \chi_C$) and (b)–(d) ratios of local spin susceptibilities (χ_i/χ_{All}; i = A, B, and C). The black stars denote the spin susceptibility of Tl(SeCN) evaluated by SQUID measurements (χ_{SQUID}). The results of $NH_4(SCN)$ and Rb(SCN) were calculated using the temerature dependence of NMR shifts in the literature [16,17].

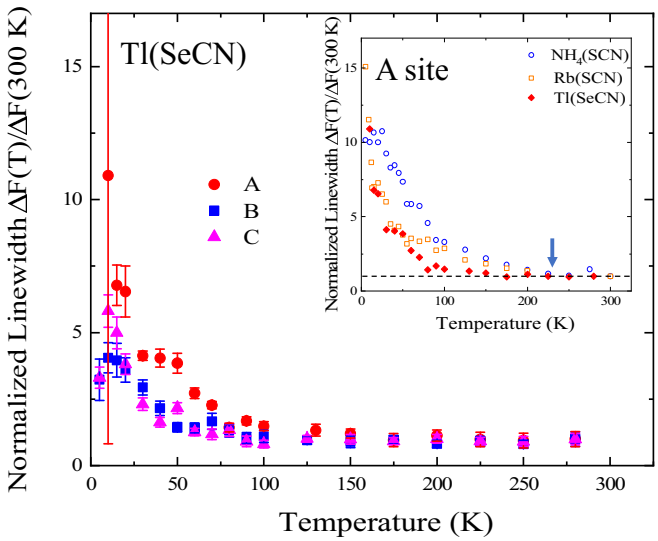

FIG. 7. Temperature dependence of the line width of the NMR shifts of the A, B, and C sites in Tl(SeCN) normalized relative to those at 300 K. The error bars indicate the uncertainty of the fits. The inset shows the temperature dependence of the line widths of the A sites in $NH_4(SCN)$ [17], Rb(SCN) [16], and Tl(SeCN).

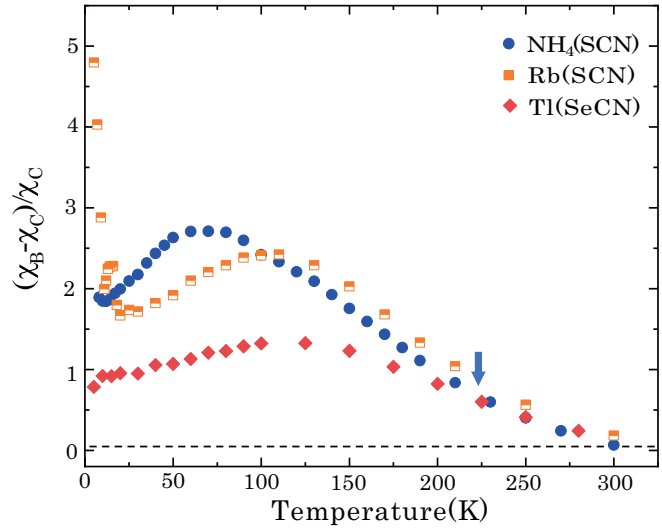

FIG. 8. Temperature dependence of χ_B/χ_C in Tl(SeCN), $NH_4(SCN)$ [17], and Rb(SCN) [16].

C. Temperature dependence of the NMR line width

Figure 7 shows the temperature dependence of the line widths of the NMR shift of the A, B, and C sites in Tl(SeCN) normalized relative to those at 300 K. The normalized line widths were 1.0 ± 0.1 in the range from room temperature to 200 K and showed similar behaviors. The line widths gradually increased below 100 K; however, this increase would not be related with T^*anomalies and would be attributed to the lattice degree of freedom rather than the charge disproportionation because there is no site and sample dependence. The inset shows the temperature dependence of the line widths of the A sites in $NH_4(SCN)$, Rb(SCN), and Tl(SeCN). In $NH_4(SCN)$ and Rb(SCN), these line widths showed an anomaly at 230 K, with the line width of the A site gradually increasing below $T^* \simeq 200$ K.

In contrast, the line widths of the B and C sites did not show anomalies at $T^* \simeq 200$ K. Because A molecules are located in a general position and are connected by inversion symmetry, the line broadening of A molecules may be attributed to the instability due to the breakage of inversion symmetry at 200 K, a finding also observed by infrared vibrational spectroscopy [18]. In Tl(SeCN), however, the line width of the A site did not increase below $T^* \simeq 200$ K and remained as sharp as the line widths of the B and C sites, suggesting that the instability was suppressed and there is no anomaly in Tl(SeCN). From the inset of Fig. 7, the anomaly of $NH_4(SCN)$ and Rb(SCN) is expected to develop at 230 K.

D. The anomaly at T^*

The behavior of Tl(SeCN) was consistent with the absence of the anomaly at $T^* \simeq 230$ K, a line broadening observed in Rb(SCN) and $NH_4(SCN)$. Optical studies reported additional absorption by the DW salt of K(SCN), and the linear thermal expansion coefficient of $NH_4(SCN)$ shows a weak maximum, which could represent a pseudogap in charge fluctuation [15,32]. However, because line broadening of the A site was not so large [16,17] and whether the disproportionation in A column develops or not was unclear, the relationships among T^*anomalies, pseudogaps, and charge disproportionation were unclear.

Figure 8 shows the temperature dependence of χ_B/χ_C in Tl(SeCN), $NH_4(SCN)$, and Rb(SCN). At room temperature, χ_B and χ_C were almost identical in all α-type salts, suggesting no charge disproportionation in the BC column of Fig. 2. Because the A sites are crystallographically equivalent and because charge disproportion is not observed in the A column at room temperature, no α-type salt shows significant charge disproportionation at room temperature.

The χ_B/χ_C ratio gradually increased with decreasing temperature. Because χ_A/χ_{All} is almost temperature independent in all α-type salts (see Sec. III B), no α-type salt showed evidence of vertical stripe disproportionation, with the increase in χ_B/χ_C indicating a develop of inhomogeneity between B and C molecules. However, the B and C molecules are crystallographically independent, such that their develop of inhomogeneity did not require a disruption of symmetry. Hence the association between anomalies at $T^* \simeq 230$ K and increases in χ_B/χ_C was unclear.

Although the χ_B/χ_C ratios of Rb(SCN)and $NH_4(SCN)$ continued to increase with decreasing temperature, the χ_B/χ_C ratio of Tl(SeCN) deviated below $T^* \simeq 230$ K and decreased at low temperatures. As the temperature of 230 K is consistent with the temperature of line width anomaly at A site, the temperature dependence of χ_B/χ_C suggests an association between T^* anomalies and the develop of inhomogeneity between B and C molecules in both DW and SC salts. The greater inhomogeneity between B and C molecules observed in Rb(SCN) and $NH_4(SCN)$ at low temperatures suggests that the line broadening in A sites corresponds to the instability of the horizontal stripe modulation. Note that the horizontal stripe modulation might not be the static modulation but the fluctuated modulation. The line broadening in A sites is not so drastic, suggesting that the inversion symmetry between A

molecules would not completely be broken and this modulation would be fluctuated.

DW and SC salts showed the development of horizontal stripe modulation below $T^* \simeq 230$ K, suggesting that the T^* anomalies, pseudogaps, and line broadening in the A column were due to horizontal stripe modulation. The instability due to horizontal stripe modulation may contribute to superconductivity.

The χ_B/χ_C of $NH_4(SCN)$ deviated from that of Rb(SCN) below 120 K and had a broad maximum around 50 K. This difference is that may have been due to the effects of NH_4^+ rotation on electronic properties. ^{2}D-NMR measurements suggested a change in motion of NH_4^+ at 130 K and an order-disorder like transition in the anion layer at 25–40 K [33]. However, the spin susceptibility of $NH_4(SeCN)$ indicated that the motion of NH_4^+ had no effect on its electronic properties [25]. A detailed study of NH_4^+ in $NH_4(SCN)$ and $NH_4(SeCN)$ is required to reveal its effect on electronic properties.

IV. CONCLUSION

The electronic structures of the metallic salt of Tl(SeCN) were compared with those of Rb(SCN) and $NH_4(SCN)$ by ^{13}C-NMR measurements, revealing relationships among T^* anomalies, pseudogaps, and line broadening. Although χ_{All} showed different temperature dependences among the DW, SC, and metallic salts, the χ_A/χ_{All} showed almost the same temperature dependence, suggesting that no α-type salts showed evidence of vertical stripe disproportionation. The NMR line width of the A sites and the χ_B/χ_C ratios in Rb(SCN) and $NH_4(SCN)$ increased, deviating from those in Tl(SeCN) below $T^* \simeq 230$ K. These results suggest the instability of the horizontal stripe modulation develops below 230 K and the pseudogap observed in an optical study is due to the formation of the horizontal stripe modulation. Below T^*, the instability of the horizontal stripe modulation could contribute to superconductivity.

ACKNOWLEDGMENTS

We thank Dr. Y. Ihara, K. Noda, and T. Kawai for helpful discussions and experimental data. This study was supported by the Hokkaido University Global Facility Center (GFC), Advanced Physical Property Open Unit (APPOU), funded by MEXT under the Support Program for Implementation of New Equipment Sharing System.

[1] J. M. Williams, A. J. Schultz, U. Geiser, K. D. Carlson, A. M. Kini, H. H. Wang, W. K. Kwok, M. H. Whangbo, and J. E. Schirber, Science **252**, 1501 (1991).
[2] H. Seo, J. Phys. Soc. Jpn. **69**, 805 (2000).
[3] M. Naka and H. Seo, J. Phys. Soc. Jpn. **83**, 053706 (2014).
[4] H. Mori, S. Tanaka, and T. Mori, Phys. Rev. B **57**, 12023 (1998).
[5] J. Merino and R. H. McKenzie, Phys. Rev. Lett. **87**, 237002 (2001).
[6] H. Mori, S. Tanaka, K. Oshima, G. Saito, T. Mori, Y. Maruyama, and H. Inokuchi, Solid State Commun. **74**, 1261 (1990).
[7] H. H. Wang, K. D. Carlson, U. Geiser, W. K. Kwok, M. D. Vashon, J. E. Thompson, N. F. Larsen, G. D. McCabe, R. S. Hulscher, and J. M. Williams, Physica C **166**, 57 (1990).
[8] H. Taniguchi, H. Sato, Y. Nakazawa, and K. Kanoda, Phys. Rev. B **53**, R8879 (1996).
[9] K. Miyagawa, A. Kawamoto, and K. Kanoda, Phys. Rev. B **56**, R8487 (1997).
[10] K. Miyagawa, A. Kawamoto, and K. Kanoda, Synth. Met. **86**, 1987 (1997).
[11] M. V. Kartsovnik, A. E. Kovalev, and N. D. Kushch, J. Phys. I France **3**, 1187 (1993).
[12] T. Sasaki and N. Toyota, Phys. Rev. B **49**, 10120 (1994).
[13] S. Uji, T. Terashima, H. Aoki, J. S. Brooks, M. Tokumoto, N. Kinoshita, T. Kinoshita, Y. Tanaka, and H. Anzai, Phys. Rev. B **54**, 9332 (1996).
[14] N. Drichko, M. Dressel, C. A. Kuntscher, A. Pashkin, A. Greco, J. Merino, and J. Schlueter, Phys. Rev. B **74**, 235121 (2006).
[15] M. Dressel, N. Drichko, J. Schlueter, and J. Merino, Phys. Rev. Lett. **90**, 167002 (2003).
[16] K. Noda, Y. Ihara, and A. Kawamoto, Phys. Rev. B **87**, 085105 (2013).
[17] Y. Ihara, K. Noda, and A. Kawamoto, Phys. Rev. B **90**, 041107(R) (2014).
[18] T. Hiejima, S. Yamada, M. Uruichi, and K. Yakushi, Physica B **405**, S153 (2010).
[19] K. Bender, I. Hennig, D. Schweitzer, K. Dietz, H. Endres, and H. J. Keller, Mol.Cryst. Liq. Cryst. **108**, 359 (1984).
[20] M. Watanabe, Y. Noda, Y. Nogami, and H. Mori, J. Phys. Soc. Jpn. **73**, 116 (2004).
[21] A. Girlando, M. Masino, J. A. Schlueter, N. Drichko, S. Kaiser, and M. Dressel, Phys. Rev. B **89**, 174503 (2014).
[22] A. Pustogow, Y. Saito, A. Rohwer, J. A. Schlueter, and M. Dressel, Phys. Rev. B **99**, 140509(R) (2019).
[23] A. Pustogow, K. Treptow, A. Rohwer, Y. Saito, M. Sanz Alonso, A. Löhle, J. A. Schlueter, and M. Dressel, Phys. Rev. B **99**, 155144 (2019).
[24] M. Maesato, Y. Kaga, R. Kondo, and S. Kagoshima, Phys. Rev. B **64**, 155104 (2001).
[25] A. Ohnuma, H. Taniguchi, Y. Takahashi, and A. Kawamoto, J. Phys. Chem. C **122**, 24321 (2018).
[26] L. I. Buravov, N. D. Kushch, V. N. Laukhin, A. G. Khomenko, E. B. Yagubskii, M. V. Kartsovnik, A. E. Kovalev, L. P. Rozenberg, R. P. Shibaeva, M. A. Tanatar *et al.*, J. Phys. I France **4**, 441 (1994).
[27] G. E. Pake, J. Chem. Phys. **16**, 327 (1948).
[28] K. Kanoda, Hyperfine Interact. **104**, 235 (1997).
[29] T. Klutz, I. Hennig, U. Haeberlen, and D. Schweitzer, Appl. Magn. Reson. **2**, 441 (1991).
[30] Y. Takano, K. Hiraki, Y. Takada, H. M. Yamamoto, and T. Takahashi, J. Phys. Soc. Jpn. **79**, 1 (2010).
[31] K. Miyagawa, A. Kawamoto, and K. Kanoda, Phys. Rev. B **62**, R7679 (2000).
[32] A. Dolbin, M. Khlistyuck, N. A. Vinnikov, and R. Basnukaeva, Low Temp. Phys. **45**, 128 (2019).
[33] S. Endo, T. Goto, T. Fukase, H. Uozaki, K. Okamoto, and N. Toyota, Phys. Rev. B **57**, 14422 (1998).